An Advanced Damage Percolation Model of Ductile Fracture

Cliff Butcher[1,*], Zengtao Chen[2], Michael Worswick[1]

[1] Department of Mechanical and Mechatronics Engineering, University of Waterloo, Canada
[2] Department of Mechanical Engineering, University of New Brunswick, Canada
* Corresponding author: cbutcher@uwaterloo.ca

Abstract

A multi-scale damage percolation model has been developed to predict fracture in advanced materials with heterogeneous particle distributions. The percolation model was implemented into a commercial finite-element code using so-called "percolation elements" to capture the complex stress- and strain-gradients that develop within the microstructure during deformation. In this approach, fracture is predicted as a direct consequence of the stress state, material properties and local conditions within the microstructure. Void nucleation, growth and coalescence models are applied for ellipsoidal voids subjected to general loading conditions. A novel void nucleation rule is employed for particle cracking based upon the particle morphology and stress state. A particle field generator has been implemented into the percolation software to generate representative particle fields based upon the field statistics obtained using x-ray micro-tomography. The percolation model was validated numerically and experimentally for an automotive-grade aluminum alloy in a notched tensile test used for material characterization.

Keywords: Void, Particle, Nucleation, Coalescence, Multi-scale

1. Introduction

The traditional approach to modeling ductile fracture involves homogenizing the microstructure of a material into a simple, equivalent geometry from which the relevant constitutive laws can be derived [1]. While attractive from a modeling perspective, critical details of the microstructure are lost in this homogenization process such as the particle size, shape, orientation, distribution and degree of clustering. Since void initiation and evolution is a highly localized phenomenon originating within heterogeneous particle clusters, these models fail to reliably predict fracture without requiring many calibration parameters. These limitations can be overcome using a damage percolation model that relies upon measured particle distributions obtained using digital imaging or x-ray micro-tomography. Micromechanical models can then be applied to each void and particle within the material to forge a direct link between local changes in the microstructure and the overall material behaviour. An advanced damage percolation model has been developed by Butcher [2] that was directly integrated into a commercial finite-element code as illustrated in Figure 1. The performance of this percolation model is evaluated by applying it to a notched tensile test specimen of AA5182 sheet. The predicted fracture strains, porosity and nucleation trends are compared and validated with the experiment data and the porosity data available in the literature.

1.1 Basics of the percolation model

The basics of the damage percolation model were established by Worswick et al. [3-4] and Chen [5] where particle fields are obtained via digital imaging techniques or micro-tomography. The particle field is then tessellated to extract the size, shape, location, and nearest neighbours of each particle and void within the field. This information is then used to re-create the particle field so that micromechanical models can be applied to each particle and void and thus predict fracture within heterogeneous particle distributions. The particles, voids and cracks are all assumed to be ellipsoidal where cracks are first formed by the coalescence of voids. The cracks are formed via a bounding box method and are subject to the same evolution laws as the voids. In the coupled

FE-percolation model of Butcher [2], the particle field is decomposed into "percolation elements" based upon the resolution of the finite-element mesh to better capture local stress and strain gradients within the microstructure. Void nucleation and coalescence occur within each percolation element with a global search for void coalescence occurring between elements at the end of each time step. The general percolation modeling strategy is outlined in Figure 2 and discussed in the subsequent sections. The interested reader is referred to [2] for additional details.

Finite-element model of a notched tensile test

Finite-elements are mapped onto a measured particle field

Micromechanical models are applied to each particle to characterize local void initiation and evolution leading to fracture
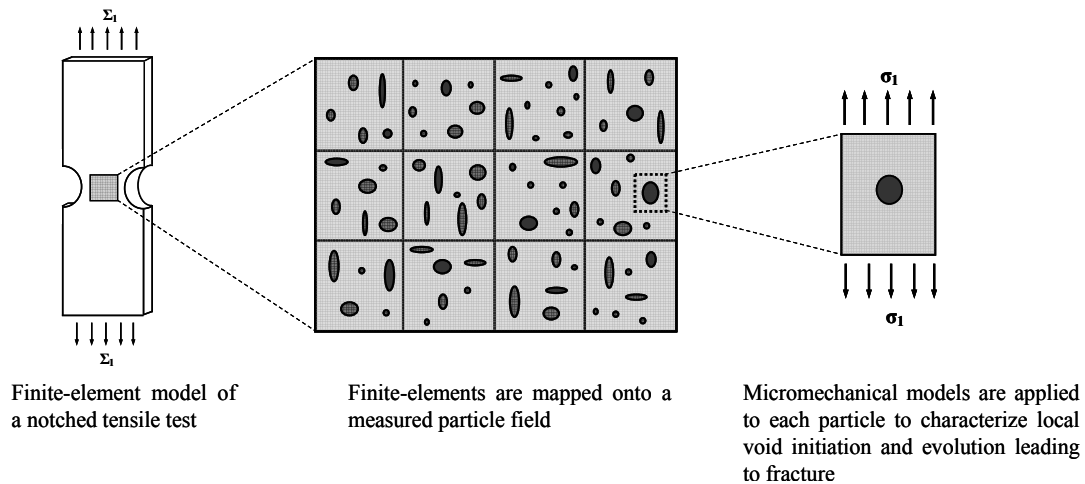
Figure 1: Multi-scale percolation model applied to a finite-element simulation of a tensile test.
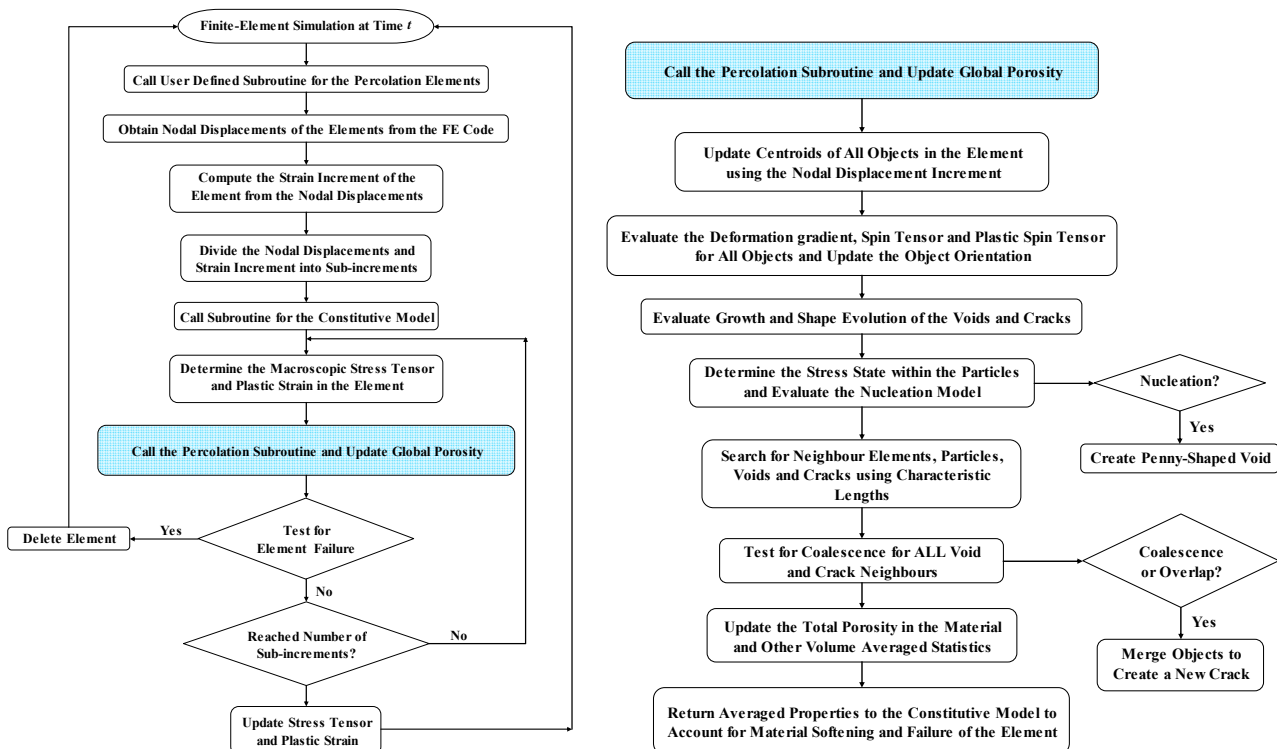
Figure 2: Flow-chart of the percolation modeling process

2. Constitutive model

The percolation material model was written as a user-defined subroutine for LS-DYNA [6] to integrate the stress state, analyze the microstructure for void evolution and return the stress tensor

and plastic strain to the finite-element program. The macroscopic stress and strain rate tensors are denoted as, Σ_{ij}, and D_{ij}, respectively. The porosity (void volume fraction), spheroidal aspect ratio and void spacing ratio are denoted as f, W, and χ, respectively. A Gurson-based yield criterion [1,7] using the modification of Ragab [8] for the q_i parameters is employed to account for material softening within the percolation element and is expressed as

$$\Phi = \left(\frac{\Sigma_{eq}}{\bar{\sigma}}\right)^2 + 2\bar{f}_d q_1(\Sigma_{hyd}, \Sigma_{eq}, n)\cosh\left(\bar{q}_2 \frac{3}{2}\frac{\Sigma_{hyd}}{\bar{\sigma}}\right) - q_1^2(\Sigma_{hyd}, \Sigma_{eq}, n)\bar{f}_d^2 - 1 = 0 \tag{1}$$

where the global porosity and average q_2 value of the voids and cracks are defined as

$$\bar{f}_d = \sum_{i=1}^{n_v} f_i^v + \sum_{i=1}^{n_c} f_i^c \qquad\qquad \bar{q}_2 = \frac{1}{\bar{f}_v}\sum_{i=1}^{n_v} f_i^v q_{2i}^v + \frac{1}{\bar{f}_c}\sum_{j=1}^{n_c} f_j^c q_{2j}^c \tag{2, 3}$$

with the subscripts v and c denote quantities for the voids and cracks, respectively, and an overbar symbol denotes a global quantity. The q_1 parameter does not require an averaging procedure since it is a function of the stress triaxiality and hardening exponent and these quantities are assumed to be homogeneous in the element. Alternatively, the q_2 parameter is a function of the void shape and stress state and will typically be different for each void and crack. The relations for the q_i parameters and the triaxiality, T, are

$$q_1 = A_0 + A_1 T + A_2 T^2 + A_3 T^3 \qquad q_2 = W^{\eta(T,n)} \qquad T = \Sigma_{hyd} / \Sigma_{eq} \tag{4-6}$$

where A_i, and η are coefficients found in Ragab [8]. The associated flow rule of the GT model yields the void growth relation that is applied for each void and crack as

$$\dot{f}_{growth} = \frac{3f(1-f)q_1 q_2 \sinh\left(q_2 \frac{3}{2}\frac{\Sigma_{hyd}}{\bar{\sigma}}\right)}{3\left(\frac{\Sigma_1 - \Sigma_{hyd}}{\bar{\sigma}}\right) + fq_1 q_2 \sinh\left(q_2 \frac{3}{2}\frac{\Sigma_{hyd}}{\bar{\sigma}}\right)} D_1^p \tag{7}$$

where Σ_1 and D_1^p are the stress and plastic strain rate in the principal loading direction.

Void coalescence is modeled using the criterion of Pardoen and Hutchinson [9] for internal necking coalescence. The onset of coalescence occurs when the following constraint is satisfied:

$$\frac{\Sigma_1}{\bar{\sigma}(1 - \kappa_{uc}\chi^2)} \geq \left((0.1 + 0.22n + 4.8n^2)\left(\frac{1-\chi}{W\chi}\right)^2 + \frac{1.24}{\sqrt{\chi}}\right) \tag{8}$$

where $\kappa_{uc} = \pi/4$ for a cubic cell. The void spacing ratio and the cell aspect ratio, λ, are defined as

$$\chi = \left(\frac{f}{\gamma}\frac{\lambda}{W}\right)^{\frac{1}{3}} \qquad\qquad \lambda = \frac{L_y}{\sqrt{L_x L_z}} \tag{9a,b}$$

where $\gamma = \pi/6$ for a cubic unit cell and L_i are its side-lengths that evolve with the applied strain. The criterion in Eq. (8) is also used to identify the onset of profuse void coalescence and failure of the percolation element. In this case, the global void aspect ratio and spacing ratios are:

$$\overline{W} = \frac{1}{\overline{f}_v} \sum_{i=1}^{n_v} f_i^v W_i^v + \frac{1}{\overline{f}_c} \sum_{j=1}^{n_c} f_j^c W_j^c \qquad \overline{\chi} = \left(\frac{\overline{f}_d \lambda_e}{\gamma \overline{W}} \right)^{\frac{1}{3}} \qquad (10,11)$$

where λ_e is the aspect ratio of the finite-element with respect to the principal loading direction.

2.1 Calibration of the void evolution and coalescence models

To ensure that the extended GT constitutive model described in the previous section is accurate for a single void, an extensive study of axisymmetric unit cells containing a dilute concentration of voids was performed with initial void aspect ratios ranging from 0.001 to 6. Each unit cell was subjected to constant triaxial loadings ranging from, $T = 1/3 - 3$, for a material with a hardening exponent of 0.1. Following the method of Ragab [8], the q_2 coefficient in Eq. (7) was calibrated for each void shape to ensure accurate predictions of the porosity. Second-order polynomials were used to describe the evolution of the void aspect ratios to high accuracy. See Butcher [2] for the complete results of this numerical study along with the calibrated coefficients for void evolution. When void growth and shape evolution are properly modeled, the coalescence strains predicted using Eq. (8) were in very good agreement with the numerical results. An example of the accuracy of the calibrated porosity trends for penny-shaped voids is shown in Figure 3a when the unit cell data is used to evaluate Eq. (7). Similarly, the predicted porosity and coalescence strains are shown in Figure 3b when the GT model in Eq. (1) is used to integrate the stress state. The good agreement of the calibrated GT model in Fig. 3b demonstrates that the predictions for void evolution and coalescence within the particle field are well represented for isolated voids.
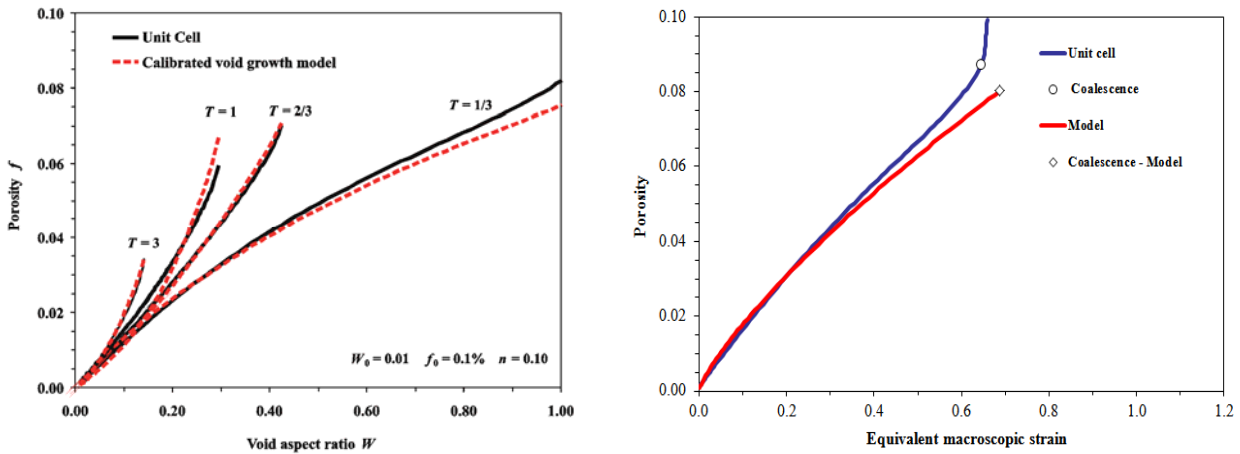
Figure 3: (a) Comparison of the porosity evolution in the unit cell and with Eq. (7) when it is evaluated using the stress state from the unit cell. (b) Comparison of the predicted void evolution and coalescence when using the GT yield criterion in Eq. (1) to integrate the stress state for a penny-shaped void in uniaxial tension.

2.2 Void nucleation

The secant-based particle homogenization scheme of Tandon and Weng [10] was implemented using the procedure of Butcher et al. [11]. Using this method, the stress state within the particles can be estimated based upon the global stress state, particle shape, volume fraction and its mechanical properties. For AA5182, the iron-rich intermetallic particles are assumed to remain elastic during deformation and nucleate voids via a penny-shaped crack in a brittle-type fracture.

Butcher et al. [11] adapted the volume-based criterion of Moulin et al. [12] for the break-up of irregularly shaped particles during rolling to ellipsoidal particles for void nucleation as:

$$\sigma_N = \frac{1}{\sqrt{\pi}} \frac{K^*_{1c}}{\sqrt[6]{V_p}} \qquad K^*_{1c} = K_{1c} \sqrt{\alpha} \qquad \alpha \approx 1 \qquad (12)$$

where K^*_{1C} is the effective critical toughness of the particle material, V_p is the average particle volume and α is a geometry parameter in the Griffith mode I crack criterion to account for various effects such as crack blunting. This criterion contains only one physically-based parameter, K_{1c}, and captures the particle size-effect where small particles nucleate at high strains while large particles nucleate at low stresses [13]. The nucleation model also predicts that brittle phases are more likely to crack than more ductile phases.

3. Generation of representative particle fields

A particle field generator was developed and implemented into LS-DYNA [6] as a pre-processor for the percolation model. The measured probability distributions from micro-tomography studies were then re-created using rejection-sampling techniques. In this work, the distributions obtained by Orlov [14] were adopted for the semi-axes, orientations, volume fractions, and spacings of the voids and particles found in AA5182. The coupling of the percolation model with a particle field generator can enable stochastic predictions of fracture by performing multiple percolation model simulations. A typical particle field with a volume of 200 μm x 200 μm x 200 μm is shown in Figure 4 where the clustering of the voids and particles is evident along with their preferential orientation along the rolling direction. The respective number of voids, Mg$_2$Si and Fe-rich particles in this volume are 447, 616, 5273, corresponding to volume fractions of 0.053%, 0.049% and 0.483%.
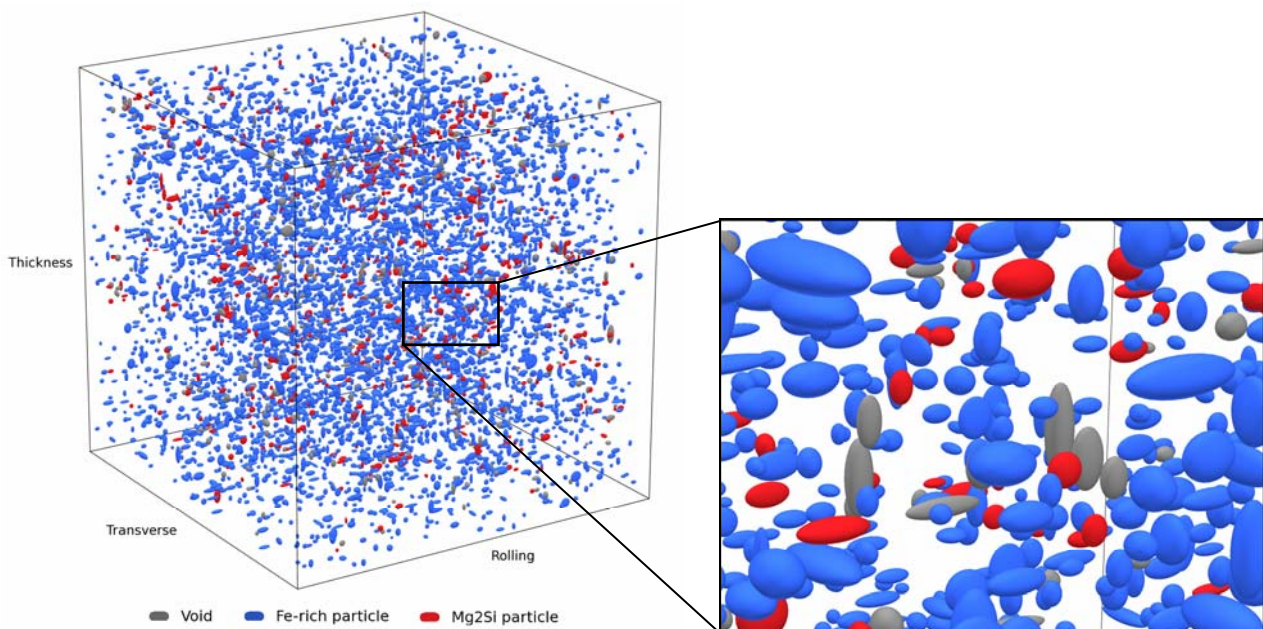
Figure 4: Generated particle field of AA5182 with a volume of 200 μm x 200 μm x 200 μm.

4. Application to a notched tensile test

Six notched tensile specimens of 1.5 mm thick AA5182 sheet with a notch radius, R, of 3 mm, gage length, L, of 12.5 mm, width, w, of 18 mm, and total sample length of 80 mm were tested to failure under quasi-static conditions. The notch ligament length is characterized using the notch ratio defined as $\rho = 2R / w = 0.25$ in this study. Fracture is characterized using both the ligament strain and axial or elongation strains. The ligament strain is representative of deformation in the region where fracture originates whereas the axial strain provides a metric for fracture based upon the bulk elongation of the material. The axial and ligament strains at fracture are defined as

$$\varepsilon_{a_f} = \ln\left(\frac{L_f}{L_o}\right) \qquad\qquad \varepsilon_{\lig_f} = \ln\left(\frac{\lig_f}{\lig_o}\right) \qquad\qquad (13,14)$$

where the initial ligament length is: $\lig_o = w_o - 2R = 12$ mm. The axial strain at failure is recorded at the appearance of a macro-crack at the notch root and not final failure since the objective of the finite-element models is to predict the formation of a macro-crack and not the subsequent tearing process. Tensile specimens with notch ratios smaller than 1/3 exhibit visible cracking at the notch root prior to fracture and the appearance of a macro crack corresponds to a sharp drop in the experimental load displacement curve [15].

4.1 Material characterization

Three tensile specimens were evaluated to characterize a Voce hardening law for AA5182 as:

$$\bar{\sigma}(\text{MPa}) = 398.1 - 275.4\exp\left[-7.631\left(\bar{\varepsilon}^p\right)^{0.905}\right] \qquad n = \frac{\bar{\varepsilon}^p}{\bar{\sigma}}\frac{d\bar{\sigma}}{d\bar{\varepsilon}^p} \qquad (15a, b)$$

with a yield stress of 122.7 MPa, and elastic moduli, $E = 65.33$ GPa and $v = 0.33$. Void nucleation in the AA5182 alloy is attributed to the iron-rich intermetallics and not the Mg_2Si particles based upon the micro-tomography study by Orlov [14]. The elastic constants of the Fe-rich particles are taken as those of steel with an elastic modulus of 200 GPa and a Poisson ratio of 0.28. It is assumed that the Fe-rich particles nucleate penny-shaped voids with an aspect ratio of 0.01 via particle cracking. The fracture toughness of the Fe-rich particles in Eq. (12) is taken as 2.15 MPa-m$^{1/2}$ based upon the measurements of Rathod and Katsuna [16].

4.2 Finite-element model

A one-eighth finite-element model of the notched specimen containing 24000 constant stress brick elements is shown in Figure 5a. For computational efficiency, only percolation elements are placed at the notch root (Figure 5b) to capture the initiation of the macro-crack while the remaining elements obey J_2 plasticity using the hardening rule in Eq. (15). The percolation model is computationally expensive and the size of the global particle field in this specific model is limited to a size of 4000 particles split into four elements. The placement of only several percolation elements at the notch root is acceptable for this specific notch geometry because deformation is

highly localized at the notch root. A previous study by Butcher and Chen [15] using a Gurson-based constitutive model has shown that the only appreciable damage occurs within this region (Figure 5c). The resulting ligament and axial strains are extracted from the FE model upon the onset of element deletion. The simulations are repeated five times for particle fields denoted P1-P5 that were generated from the tomography data of Orlov [14].

| (a) | (b) | (c) |
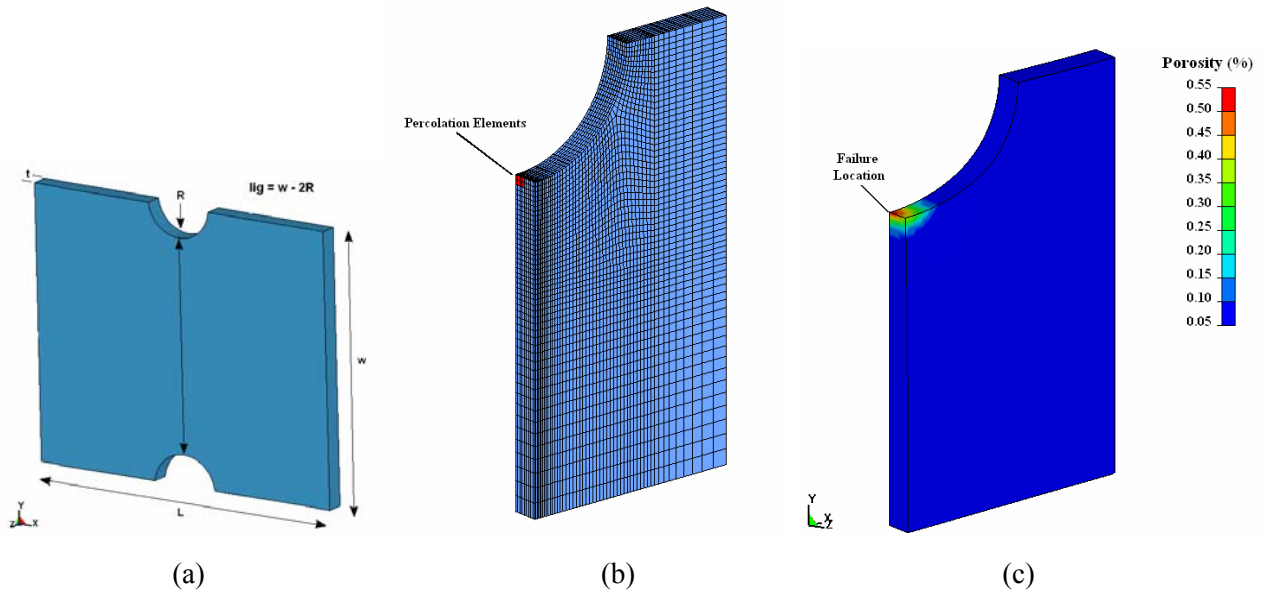
Figure 5: (a) Typical notch geometry. (b) 1/8th FE mesh showing percolation elements and (c) Porosity distribution obtained by Butcher and Chen (2011) using a traditional GT damage model.

5. Results and discussion

The predictions of the percolation model for the axial and ligament strain with the experimental values are shown in Figures 6a and 6b. The fracture strains are presented as 95% confidence intervals due to the stochastic nature of the percolation model. Although only five particle fields were considered, the variation in the axial strain predicted by the percolation model is comparable to the experimental variation.

The predicted porosity distributions of the five particle fields considered are shown in Figure 7a. All of the particle fields are in excellent agreement with the experimental porosity data of [14] at a plastic strain up to 0.10 and show generally good agreement at the higher strain levels. All of the particle fields considered, P1-P5, exhibit the same behaviour where deformation is relatively homogenous until the commencement of void nucleation at higher strains. The start of nucleation is followed by localized coalescence which promptly sweeps throughout the particle field causing failure. The fracture porosities are also in good agreement with the metallographic observations of Smerd et al. [17] who reported failure porosities on the order of 0.3%.
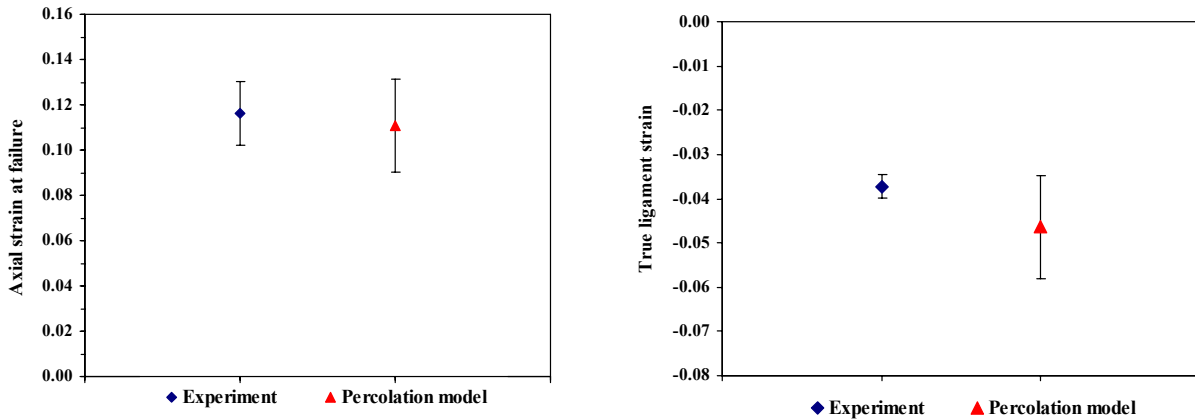
Figure 6: (a) Comparison of the experimental and predicted 95% confidence intervals for the true axial strain at failure and (b) true ligament strain.

The number of voids in the particle field is representative of void nucleation and the experimental and numerical predicted values are presented in Figure 7b. The predicted number of voids in each of the particle fields are in are in very good agreement with the experimental measurements of Orlov [17]. The convergence of the nucleation predictions demonstrates that only several particle fields are required to obtain the general trends. The porosity and fracture strains in the previous figures are expected to exhibit the most variation because they are related to coalescence which is strongly dependent upon the local microstructure. This agreement with the experimental nucleation trends is very encouraging for the physical foundation of both the percolation and the nucleation models.
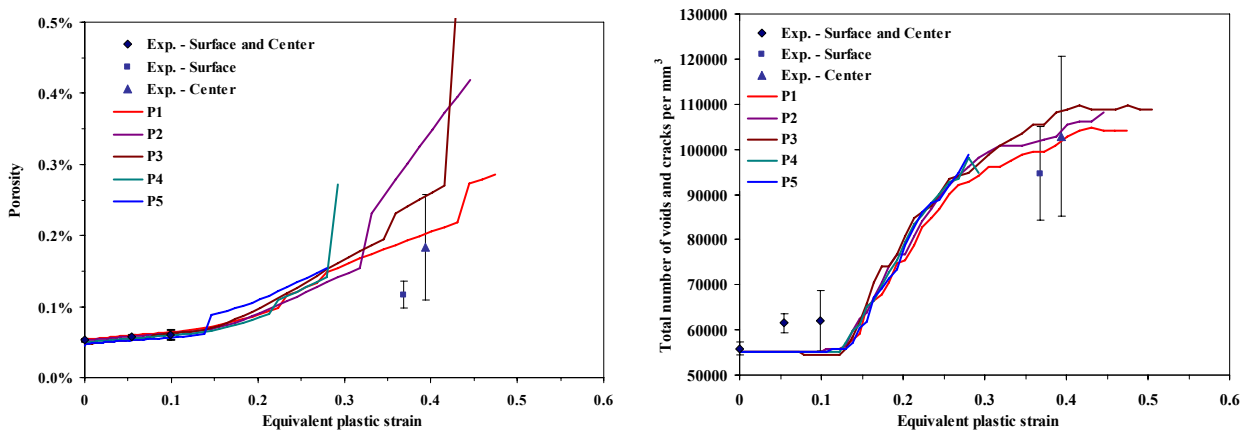
Figure 7: (a) Comparison of the predicted porosity and (b) total number of voids and cracks in the center of the notch root. The experimental tomography data is from [17] using a standard tensile specimen.

The average principal stress in the particles upon cracking (void nucleation) is shown in Figure 8a. Large particles crack at low stresses early in the deformation process while the smaller particles do not nucleate until the later in the deformation process. From this result, the stress required to fracture an Fe-rich particle is about 950 MPa. A strain-based nucleation criterion can also be developed by comparing the average volume of a broken particle to the global plastic strain

at which it nucleated as shown in Figure 8b. All of the particle fields display the well-known behaviour that small voids will nucleate only at high strains while larger particles display a negligible size effect and have a near constant nucleation stress or strain. Orlov [14] experimentally observed that no particles that had a volume smaller than 17.8 μm^3 nucleated a void and this is in accordance with the predictions of the model.
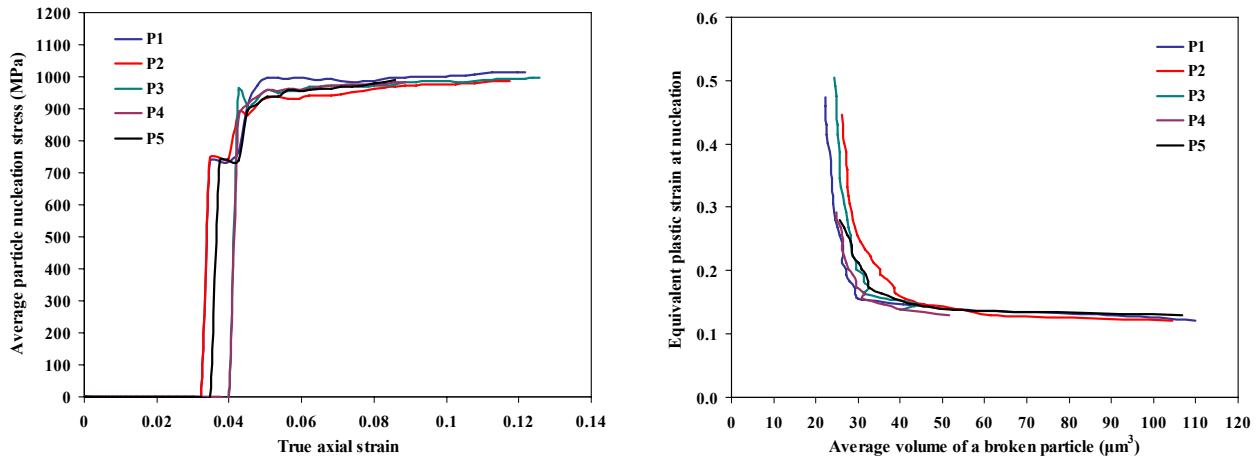
Figure 8: (a) Comparison of the average maximum principal stress in the particles at nucleation and (b) equivalent plastic strain in the matrix upon nucleation.

6. Summary

The complete damage percolation model was used to predict fracture and damage evolution in a notched tensile sheet specimen of AA5182 sheet. Representative particle distributions were created and mapped to the percolation elements located at the notch root where fracture initiates in the sample. The fracture strain, porosity, and nucleation predictions of the model are in very good agreement with the experiment data of Orlov [14]. No calibration or adjustable parameters were employed in the model and its good predictions of the experiment data attest to the strong physical foundation of the model. Fracture is a sole consequence of the stress state, material composition and the particle distribution. The main advantages of the present percolation model are that it is directly coupled into a finite-element code, contains a particle field generator as a preprocessor, and rests upon a minimum of assumptions regarding void evolution. At present, the main limitation of the model is its significant computational cost. The next phase of development of the percolation model will address this limitation and involve a large-scale application to a practical metal forming operation.

References

[1] Gurson, A.L. (1977). Continuum theory of ductile rupture by void nucleation and growth – Part I. Yield criteria and flow rules for porous ductile media. *J. Eng. Mech. Tech.* **99**, 2-15.
[2] Butcher, C. (2011). A multi-scale damage percolation model of ductile fracture. Ph.D. thesis, University of New Brunswick, Canada: http://dspace.hil.unb.ca:8080/handle/1882/35391

[3] Worswick, M.J., Pilkey A.K., Thomson C.I.A., Lloyd D.J. and Burger G. (1998), Percolation damage predictions based on measured second phase particle distributions, *Micro. Sci.*, 507-514

[4] Worswick, M.J., Chen Z.T., Pilkey A.K., Lloyd D., Court S. (2001). Damage characterization and damage percolation modeling in aluminum alloy sheet. *Acta Mater.* **49**, 2791-2803.

[5] Chen, Z.T. (2004). The role of heterogeneous particle distribution in the prediction of ductile fracture. Ph.D. Thesis, University of Waterloo, Canada.

[6] Hallquist, J.O. (2006). LS-DYNA Theory Manual. Livermore Software Technology Corp.

[7] Tvergaard, V. (1981). Influence of voids on shear band instabilities under plane strain conditions. *Int. J. Frac.* **17**, 389-407.

[8] Ragab, A.R. (2004). Application of an extended void growth model with strain hardening and void shape evolution to ductile fracture under axisymmetric tension. *Eng. Fract. Mech.* **71**, 1515-1534.

[9] Pardoen, T., Hutchinson, J. (2000). An extended model for void growth and coalescence. *J. Mech. Phys. Solids* **48**, 2567-2512.

[10] Tandon, G.P. and Weng, G.J.: Average stress in the matrix and effective moduli of randomly Oriented composites. *Compos. Sci. Tech.* **27**, 111-132 (1986)

[11] Butcher. C., Chen, Z.T. and Worswick, M.J. (2013). Integration of a particle-based homogenization theory into a general damage-based constitutive model to improve the modelling of void nucleation to coalescence. *Acta Mech.* **224**, 139-156.

[12] Moulin N., Jeulin D., Klöcker H., (2009). Stress concentrations in non-convex elastic particles embedded in a ductile matrix. *Int. J. Eng. Sci.* **47**, 170–191

[13] Thomason, P. (1990). *Ductile fracture of metals*. Pergamon Press Inc., Oxford.

[14] Orlov, O. (2006). A three-dimensional damage percolation model. Ph.D. Thesis, University of Waterloo, Waterloo, Ontario, Canada

[15] Butcher, C., Chen, Z.T. (2011). Characterizing void nucleation in a damage-based constitutive model using notched tensile sheet specimens. *Theor. Appl. Frac. Mech.*, **55**, 140-147.

[16] Rathod, M.J., Kutsuna, M. (2004). Joining of Aluminum Alloy 5052 and Low-Carbon Steel by Laser Roll Welding. *Welding Research*, January, 16-26.

[17] Smerd, R., Winkler, S., Salisbury, C., Worswick, M., Lloyd, D. and Finn, M. (2005). High strain rate tensile testing of automotive aluminum alloy sheet. *Int. J. Impact. Eng.* **32** 541-560.